IEEE Access
Multidisciplinary | Rapid Review | Open Access Journal

Received November 21, 2019, accepted December 30, 2019, date of publication February 6, 2020, date of current version February 17, 2020.

Digital Object Identifier 10.1109/ACCESS.2020.2972080

Investigation of Device Dimensions on Electric Double Layer Microsupercapacitor Performance and Operating Mechanism

FARHEEN NASIR AND MOHAMMAD ALI MOHAMMAD
School of Chemical and Materials Engineering, National University of Sciences and Technology, Islamabad 44000, Pakistan
Corresponding author: Mohammad Ali Mohammad (dr.ali@scme.nust.edu.pk)

This work was supported by NUST Internal Research funding.

ABSTRACT Electric Double Layer Capacitor (EDLC) holds the highest share of commercial supercapacitor market. However, it has been proven that current Helmholtz, Gouy-Chapman and Stern models do not provide comprehensive explanation for energy storage mechanism in EDLC. In this work the effects of interdigitated EDLC design on capacitance of flexible laser scribed interdigitated microsupercapacitor (LSG-MSC) are studied. Three design parameters are tested, (1) current collector-electrode interaction, (2) electrode aperture, and (3) distance between parallel electrodes. Noticeable change was observed in the total capacitance upon change in LSG-MSC design which was analyzed in detail using cyclic voltammetry, electrochemical impedance spectroscopy and electrostatic simulation using COMSOL Multiphysics. It was found that in addition to electric double layer capacitance, an electric field was generated between electrodes and between electrode and current collector which led to small electrostatic capacitance between them. This electric field was also found to cause disturbance in double layer formation at the electrode thus causing change in the overall capacitance as the design parameters were varied.

INDEX TERMS COMSOL multiphysics, electric double layer capacitor, flexible electronics, laser scribing, microsupercapacitor.

I. INTRODUCTION

The concept of electric double layer capacitance was first discovered by Hermann von Helmholtz in 1853 [1]. He stated that for a charged electrode in an electrolytic solution, another electrode is formed at the electrode/electrolyte interface by ions from the electrolyte solution, and the two electrodes are separated by only a few Angstroms as shown in Fig. 1(a). The double layer is considered to be a molecular capacitor with distance between the plates in Angstroms thus having very high specific capacitances. However, this model was only valid for solutions with very high electrolyte concentration.

In 1910 and 1913 respectively, Guoy and Chapman gave separate theories for electric double layer formation in dilute solutions [2], [3]. The combination of their respective explanations became known as the Gouy-Chapman model. In the combined model, exchange of counter ions between the layer of adsorbed ions (stern layer) and the bulk of the solution is also considered. The effect of thermal motion and coulomb forces on counter ion distribution is also described, as shown in Fig. 1 (b).

In 1923, Stern described two regions of ion distribution using Helmholtz and Gouy-Chapman models. The inner region, which was initially described by Helmholtz, is called the compact/Stern layer and the diffused ions which form a loose layer in the outer region are called Gouy-Chapman layer as shown in Fig. 1(c). The two regions are also called inner Helmholtz plane (IHP) and outer Helmholtz plane (OHP) respectively. Total capacitance C_{dl} for the EDLC is a combined effect of capacitances from IHP (Stern layer capacitance C_s) and OHP (capacitance due to diffusion layer C_{diff}).

$$\frac{1}{C_{dl}} = \frac{1}{C_S} + \frac{1}{C_{diff}}$$

Practical EDLC has a high surface area porous electrode and the electric double layer behavior is affected by several parameters including space constraints of the pores, electrolyte resistance, mass transfer path, inter-electrode distance,

The associate editor coordinating the review of this manuscript and approving it for publication was Yunfeng Wen.

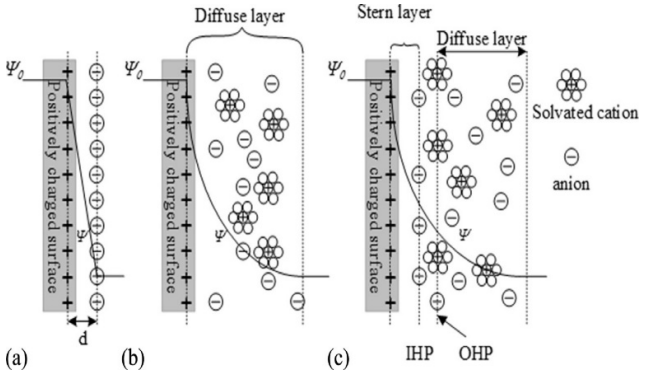

FIGURE 1. Double layer models by: (a) Helmholtz, (b) Gouy-Chapman and (c) Stern [7]. Copyright 1994 Published by Elsevier B.V. Reprinted with permission.

wettability of porous electrode etc., thus it cannot be fully described by the models shown in Fig. 1 [4]–[6].

During the past two decades EDLCs have seen a surge in development and commercialization due to high demand from consumer electronics such as laptops, mobile phones and even electric vehicles. With such high demand it is important to understand the working mechanism of EDLC in order to utilize its full potential. Extensive experimental and simulation studies have been done to investigate the effect of electrode [8]–[13] and electrolyte material [14]–[17] on the performance of EDLC. However, Stern model is still the standard model used for prediction of EDLC behavior even though it does not take into account the various electrode and electrolyte factors effecting the total capacitance.

Two most commonly used geometries for EDLC are stacked and interdigitated electrodes. While stacked EDLC are easy to fabricate, they have significantly less energy density compared to their counterparts as well as being incompatible with on-chip microsystems. Interdigitated microsupercapacitors (MSC) on the other hand, have very fast charging/discharging, long life time and high power density and operating voltage. However, despite the clear superiority of interdigitated MSC over stacked geometry, as well as experimental evidence suggesting change in total capacitance of MSC by variation in device dimension [18], [19] there has been no thorough investigation to study this effect in depth to the best of our knowledge.

MSCs are commonly prepared using photolithography [20]–[23]. However, recently laser scribing has emerged as an inexpensive and facile method for the fabrication of high performance MSC on flexible substrates [24]–[26]. In this case a high energy laser causes photothermal or photochemical reaction on the surface of a polymer and converts it into conductive carbonaceous material commonly referred to as laser scribed graphene (LSG). By controlling the movement of laser on the polymer surface we can make conductive paths in our desired patterns. Furthermore, the carbonized material produced by laser scribing is highly porous which makes it an ideal candidate for EDLC electrodes.

Our group has previously fabricated laser scribed supercapacitors [27] as well as rGO based strain sensors [28] based on the principle of laser scribing. In this work, we have investigated the effect of device dimensions on the performance of flexible laser scribed MSC. We have also performed electrostatic study using COMSOL Multiphysics to investigate electric field produced between electrodes and between electrode and current collector. Lastly, experimental and simulation results have been compared to find correlation between change in total capacitance of LSG-MSC and electric field.

II. METHODS

Three set of MSCs (Fig. 2) were fabricated using laser scribing on flexible polyimide substrate. The laser used had wavelength of 410nm and experiments were performed with 106mW laser power. The dominant mechanism for formation of LSG was determined to be photothermal reduction [29]. In this case, laser irradiation causes high temperature, in the range of ∼2500-3000°C, at the surface of polyimide which provides enough energy to break C-O, C = O and C-N bonds and leads to the formation of conductive C-C bonds at the surface.H3PO4/PVA polymer gel electrolyte was used which was synthesized according to literature [18]. MSC1 was designed to study the relationship between electrode and current collector distance. In MSC2 the authors have studied relationship between two overlapping electrodes and how the area of overlapping (also called aperture) affects the capacitance of EDLC, while in MSC3 the effect of inter-electrode distance on total device capacitance was studied. Detailed design information and hypothesis about each set of MSC can be found in supplementary information.

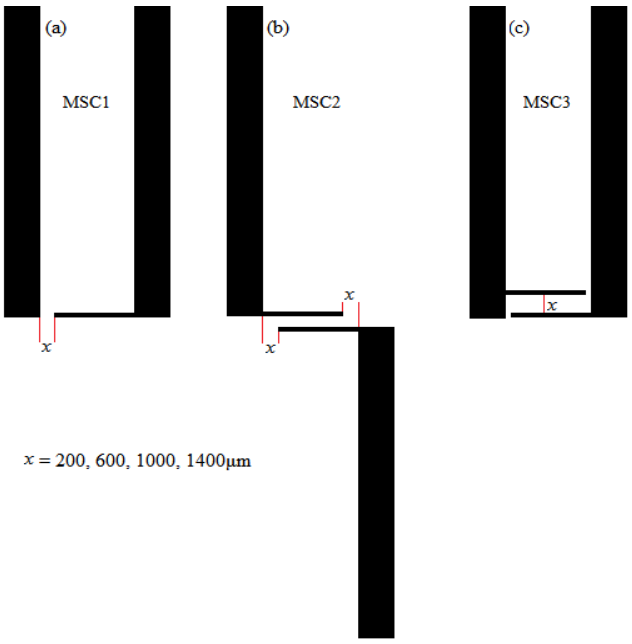

FIGURE 2. (a) MSC1 (varying electrode-current collector distance). (b) MSC2 (varying MSC aperture). (c) MSC3 (varying inter-electrode distance).

Each set of MSC was also simulated to study the electrostatic fields being produced. First, 2D structures were

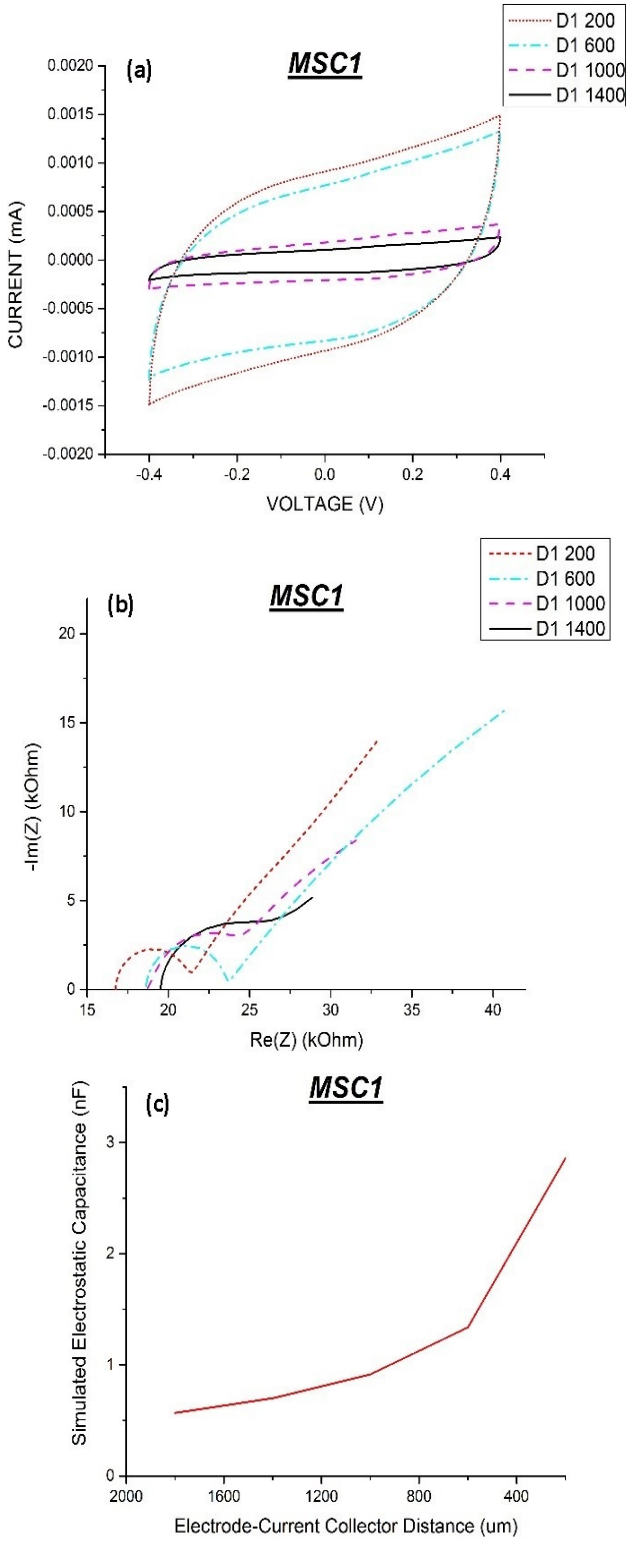

FIGURE 3. (a) Cyclic Voltammogram, (b) Nyquist plot, and (c) simulated electrostatic capacitance vs. electrode-current collector distance for MSC1.

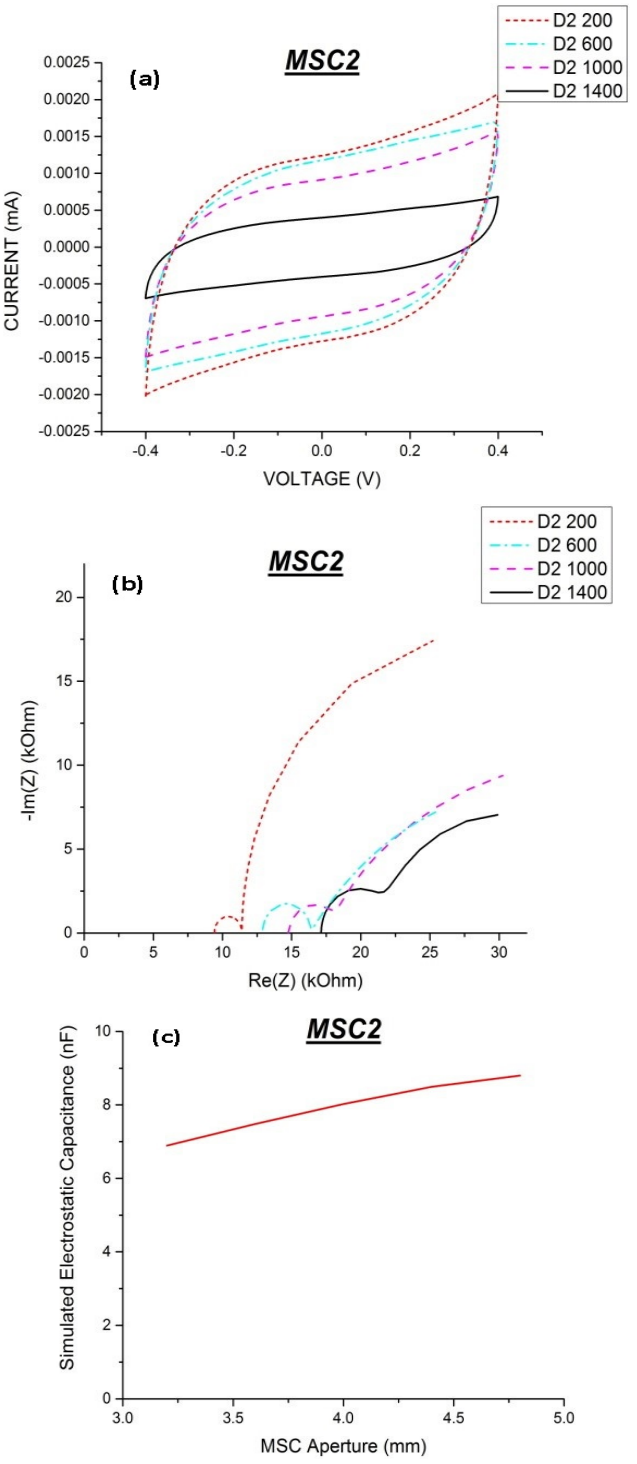

FIGURE 4. (a) Cyclic Voltammogram, (b) Nyquist plot, and (c) simulated electrostatic capacitance vs. electrode-current collector distance for MSC2.

designed in COMSOL Multiphysics using parameters listed in table SI. Note that all the design and material parameters used for simulation were the same as that for fabricated MSCs. Next, the designed supercapacitors were studied using the AC/DC (electrostatics) physics functionality in COMSOL Multiphysics. Maxwell capacitance was noted for each structure as well as the direction and strength of electric field lines, electric potential contour between current collector and electrode and between two electrodes.

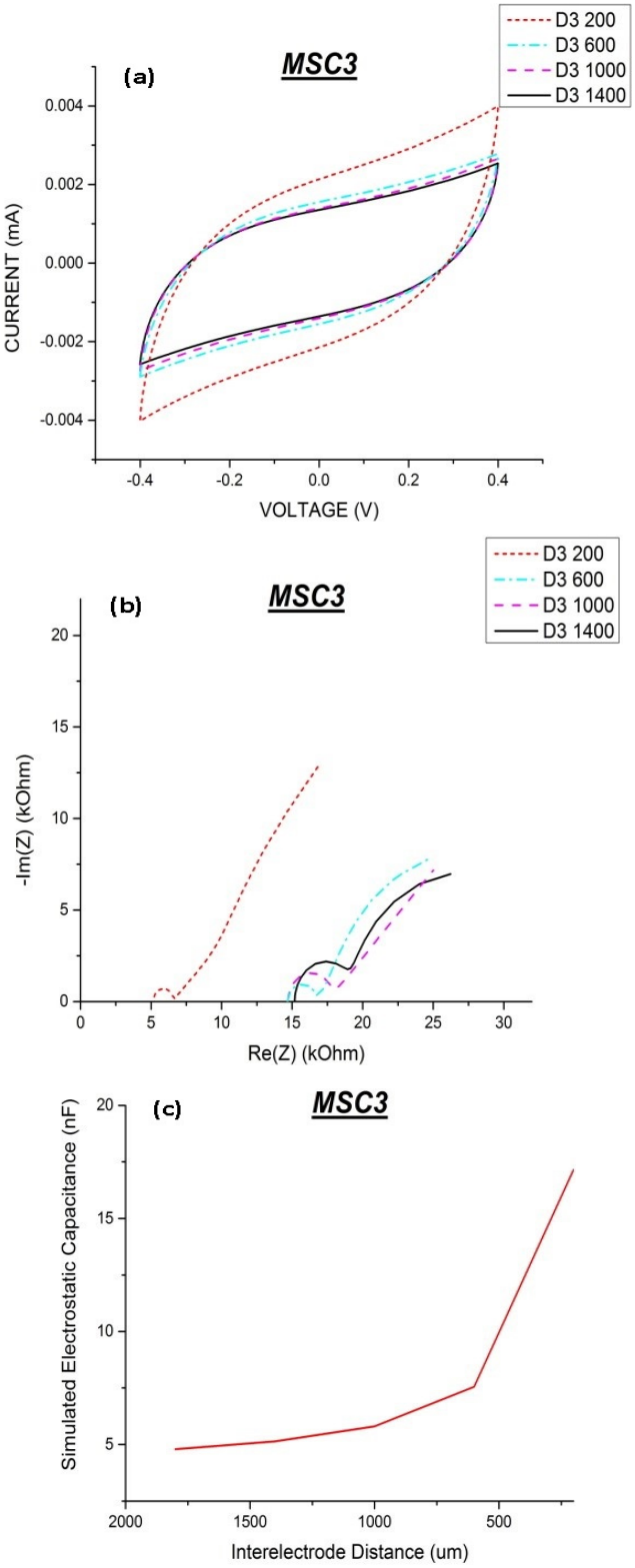

FIGURE 5. (a) Cyclic Voltammogram, (b) Nyquist plot, and (c) simulated electrostatic capacitance vs. electrode-current collector distance for MSC3.

III. RESULTS AND DISCUSSION

The fabricated MSCs first underwent material characterization to confirm the formation of laser scribed graphene and to determine its height relative to polyimide sheet. For this purpose, X-ray Diffraction (XRD), Scanning Electron Microscopy (SEM) and Optical Profilometry were performed. The synthesized electrolyte was characterized using Fourier Transform Infrared Spectroscopy (FTIR). These results are discussed in supplementary information (Fig. SI-SV).

Next, electrochemical characterization was done using cyclic voltammetry (CV) and electrochemical impedance spectroscopy (EIS) to determine change in total capacitance with respect to device dimensions. Fig. SVI shows typical Nyquist plot for EDLC with parameters identifying device performance such as resistances R_A, R_{AB}, R_B, R_C and slope of line BC (k_{BC}).

A. MSC1

Fig. 3a and 3b show the cyclic voltammogram and Nyquist plot for MSC1 respectively. From Fig. 3a it was observed that as the distance between electrode and current collector increased from 600μm to 1000μm, there was a sharp decrease in total capacitance of the device. Nyquist plot of Fig. 3b shows that this was due to increase in polarization resistance (R_{AB}) as explained in supplementary information and shown in table SII.

R_A is defined as the sum of electrolyte resistance in pores of electrode and electrode resistance [18], [30]. For MSC1 the value of R_A increased as distance between current collector and electrode was increased. This might be due to electric field being produced between the current collector and edge of electrode which induced an electrostatic capacitance between the two. As the distance between the electrode and current collector increased, the electric field strength decreased causing increase in R_A. Furthermore, as the distance increased from 200μm to 600μm, R_A increased more than 2kΩ after which it experienced some saturation, possibly due to sharp decrease in electric field. Since electric field was experienced only at the edge of the electrode, its effect on electrolyte and electrode surface resistance is not pronounced and thus it was not the dominant factor for decrease in capacitance for MSC1. Increase in R_A was also not as pronounced in MSC1 as in MSC2 and MSC3 for the same reason. Note that the surface area of device, electrolyte concentration and laser parameters were kept constant for all MSCs so as not to cause change in capacitance due to double layer effect.

R_{AB} is often referred to as charge transfer resistance attributed to length of ion diffusion pathway between two electrodes [6], [18], [31]–[33] or as polarization resistance which is defined as resistance encountered by the electrolyte ions during penetration inside the electrode [30], [34], [35]. For MSC1, R_{AB} was hypothesized to be polarization resistance since the MSC was designed to have only one electrode. R_{AB} also increased as the distance between electrode and current collector increased. The authors suggest that electric field between the edge of electrode and current collector caused the surface resistance of electrode to decrease [36], [37] thus decreasing the polarization resistance by providing less resistive path to ion transport inside pores of the electrode.

As distance between current collector and electrode increased, the electric field decreased leading to increase in electrode surface resistance and consequently increase in polarization resistance. At distance greater than 600μ m the authors observed significant increase in R_{AB} which in turn caused decrease in capacitance, as evident from cyclic voltammetry curves.

The next parameter analyzed was the slope of line BC (k_{BC}). The parameter k_{BC} is defined as the ratio between time constants τ_D and τ_{RC}, ($k_{BC} = \tau_D / \tau_{RC}$) [38], where

$$\tau_D = \frac{L^2}{D}$$
$$\tau_{RC} = (R_{EB} + R_D)^* C_{diff}$$

τ_{RC} corresponds to the behavior of an ideal RC circuit with resistance ($R_{EB} + R_D$) in series with a capacitor with total differential capacitance C_{diff}. In the case of EDLC, R_{EB} and R_D are defined as bulk electrolyte resistance and diffuse layer resistance respectively. The parameter τ_D is the time constant corresponding to the diffusion of electrolyte ions and depends on the total length covered by the electrolyte (L) and the diffusion coefficient (D) of the electrolyte [38]. It has been proven that as electric field increases, the diffusion coefficient of electrolyte decreases due to highly resistive path experienced by the electrolyte ions in the region of electric field [39]. When the electrode was placed close to the current collector (distance $\leq$200μm) the electric field experienced by it was very large. This high electric field caused decrease in the diffusion coefficient (D) which in turn increased τ_D and consequently caused high k_{BC}. As the distance between the current collector and electrode increased, D increased and resulted in decreased value of τ_D and k_{BC} as shown in table SII. It should be mentioned that though the electric field strength decreases drastically at distances larger than 600μm, it is still present and is strong enough to effect D.

It should also be noted that the EIS results from this work do not show straight line at lower frequencies corresponding to behavior of ideal RC circuit due to highly porous nature of LSG electrode.

Next, COMOL based simulation was used to test the electric field being produced between current collector and electrode and the resulting electrostatic capacitance between the two. The authors found that at distance smaller than 600μm there was drastic increase in electrostatic capacitance of the device (Fig. 3c and table SIII). As mentioned above, there was also a sharp change in R_A at these distances which led us to conclude that R_A is directly influenced by electric field between electrode and current collector .

B. MSC2

Fig. 4a shows the cyclic voltammogram for MSC2. It is evident from the graph that there is almost linear decrease in capacitance as the aperture of the two electrodes decreases from 4.8mm to 3.6mm from MSC2-200 to MSC2-1400 respectively. This was found to be due to increase in electric field inside the MSC which decreased linearly as aperture decreased. Cause of the increase in capacitance is explained in depth using Nyquist plot (Fig. 4b) and COMSOL simulations (Fig. 4c).

From Nyquist plot of Fig. 4b we observed increase in R_A, R_{AB} and slope of line BC (k_{BC}) as the aperture decreased while simultaneously the total capacitance decreased as evident from cyclic voltammogram of Fig. 4a. The percent change in aperture was found to be 33.33% while the change in R_A and R_{AB} was 45% and 66.2% from MSC2-200 to MSC2-1400 respectively (table SIV). This implies that in addition to longer ion diffusion path for MSC2-1400 there was another force causing increase in R_A and R_{AB}. From simulation it was observed that electrostatic field between the two electrodes decreases 17.6% in strength as the aperture decreased from MSC2-200 to MSC2-1400. Accounting for $\pm$5% variation in experimental and simulation results, it can be estimated that electrostatic field between the two electrodes causes change in R_A and R_{AB} under the same effects as mentioned for MSC1. Change in k_{BC} from MSC2-200 to MSC2-1400 is $\sim$10% larger than that for MSC1. This is due to larger area covered by electric field for MSC2 than for MSC1. However, for MSC2, the ion diffusion pathway between two electrodes increases from MSC2-200 to MSC2-1400 which also plays a role to decrease total capacitance of the system as explained by Kim *et al.* [18], while this effect was not present for MSC1.

Simulation results found similar trend for electric field, i.e., there was no sharp change in electric field between the electrodes. This was because the distance between electrodes remained constant while the total area which experienced electric field changed, causing change in electrostatic capacitance as shown in Fig. 4c.

C. MSC3

For MSC3 the authors noted the change in total capacitance due to change in inter-electrode distance. Fig. 5a shows the cyclic voltammogram of MSC3. As the inter-electrode distance increased from 200μm to 600μm, we observed sharp decrease in capacitance, similar to that for MSC1. This has been previously attributed to high electric field between the electrodes.

As is evident from Nyquist plot (Fig. 5b) and table SVI, the values measured for R_A are significantly smaller for MSC3-200 than those for MSC1 and MSC2. Similar results were obtained by Kim *et al.* who attributed it to smaller ion diffusion pathway between the electrodes as the distance between them decreased [18]. While this effect is plausible, the increase in R_A and consequent decrease in total capacitance should be somewhat linear as the electrodes moved apart. Instead, as noted by us and Kim *et al.*, there was a sharp decrease in capacitance as the distance between the electrodes increased to 600μm. From Nyquist plot of Fig. 5b it was observed that as inter-electrode distance increased beyond MSC3-600 the value of R_A increases by a very small amount ($\sim$500Ω for this work). This led us to suggest that at small inter-electrode distance, large electric field is present

TABLE 1. Summarized results from experimental and simulation studies. .

DESIGN / CAUSE FOR CHANGE IN	MSC1	MSC2	MSC3
R_A	Change in electric field.	Change in electric field and ion diffusion pathway between electrodes.	Change in electric field and ion diffusion pathway between electrodes.
R_{AB}	Change in electric field.	Change in electric field and ion diffusion pathway between electrodes.	Change in ion diffusion pathway between electrodes.
k_{BC}	Change in electrolyte diffusion coefficient due to electric field.	Change in electrolyte diffusion coefficient due to electric field.	Change in electrolyte diffusion coefficient due to electric field.
Total Capacitance	Change in R_{AB}.	Linear change in electric field between electrodes.	Change in R_A.

between electrodes causing electrostatic capacitance between them as well as enhancing double layer capacitance by causing decrease in R_A. The effect of electric field decreases drastically when inter-electrode distance is increased beyond 600μm causing significant decrease in electrostatic and electric double layer capacitances. This effect has also been shown by simulation (Fig. 5c). We observed that for MSC3 the dominant factor for decrease in capacitance was increase in R_A, which was due to sharp decrease in electric field at inter-electrode distance greater than 600μm.

The resistance R_{AB} increases linearly from MSC3-200 to MSC3-1400, suggesting that in this case it is dominated by decrease in ion diffusion length. k_{BC} also increases linearly from MSC3-200 to MSC3-1400 and can be explained by the same reasoning as that for MSC1.

Simulation results for MSC3 are similar to those for MSC1 except that the strength of electric field and consequently electrostatic capacitance was much greater for the former. This was because the total area experiencing electric field is much higher for MSC3. At inter-electrode distance greater than 600μm the electrostatic capacitance between two electrodes experienced very small decrease. Same effects were observed for R_A and total capacitance obtained, which led us to conclude that electric field produced between two electrodes is directly responsible for change in total capacitance between them for MSC3.

IV. DISCUSSION

Table 1 shows the summarized results of the above discussion. In this work we have studied the effect of design parameters for microsupercapacitor on the total capacitance of the device. The authors did not evaluate the effect of electrode width on total capacitance as it is clear that increase in electrode width would cause increase total capacitance due to increased surface area[19].

This work can be used as a guideline for designing microsupercapacitor with maximum attainable capacitance. Based on well-known principles, it is expected that as the distance between electrodes and current collector decreases the capacitance will continue to increase. Simulation results show that at electrode-current collector distance in order of few hundred nanometers, the electrostatic capacitance increases to several microfarads. This suggests that the effect of the electric field on double layer formation (via change in electrolyte diffusion coefficient) as well as electrostatic capacitance cannot be ignored for on-chip microsupercapacitors and understanding its mechanism is important for designing high performance on-chip microsupercapacitors.

V. CONCLUSION

We have shown through experiment and simulation that the total capacitance of interdigitated microsupercapacitor is heavily dependent on the distance between electrodes and between electrode and current collector.

- Within the range of dimensions studied in this work, the optimal distance between electrodes and current collector as well as between two electrodes for maximum capacitance was found to be 600μm or less.
- It was also found that the aperture of MSC also influenced total capacitance of the device and should be kept as large as possible.
- It was concluded that these results were due to electric field being generated between conductors (current collector and electrodes) which resulted in electrostatic capacitance between them. The generated electric field also caused change in diffusion coefficient of electrolyte thereby causing change in the formation of electric double layer on surface of the electrode.
- Additionally, from Nyquist plots of all MSCs it was found that the total device capacitance is dependent on the value of resistances R_{AB} and R_A as well as on the electric field generated between electrodes and between electrodes and current collector.
- Lastly, it was found that electric field between conductors and change in ion diffusion pathway between

electrodes were the major factors causing change in total capacitance of the microsupercapacitor.

ACKNOWLEDGMENT

The authors wish to acknowledge Dr. A. Akram, Dr. U. Manzoor, and T. Malik from the National University of Sciences and Technology (NUST), for their useful discussions and assistance with electrolyte synthesis and electrochemical measurements. They also thank Prof. A. Baig from the National Center for Physics (NCP) and his team for measurement of laser system and to lab technicians late S. Ud Din, H. M. Riaz, and K. Shahzad for assistance in SEM, FTIR, and XRD analysis, respectively.

REFERENCES

[1] H. Helmholtz, "Ueber einige Gesetze der Vertheilung elektrischer Ströme in körperlichen Leitern, mit Anwendung auf die thierisch-elektrischen Versuche (Schluss.)," *Ann. Phys. Chem.*, vol. 165, no. 7, pp. 353–377, 1853.

[2] M. Gouy, "Sur la constitution de la charge électrique à la surface d'un électrolyte," *J. Phys. Theor. Appl.*, vol. 9, no. 1, pp. 457–468, 1910.

[3] D. L. Chapman, "LI. A contribution to the theory of electrocapillarity," *London, Edinburgh, Dublin Phil. Mag. J. Sci.*, vol. 25, no. 148, pp. 475–481, Apr. 1913.

[4] P. Sharma and T. Bhatti, "A review on electrochemical double-layer capacitors," *Energy Convers. Manage.*, vol. 51, no. 12, pp. 2901–2912, Dec. 2010.

[5] B. Akinwolemiwa, C. Peng, and G. Z. Chen, "Redox electrolytes in supercapacitors," *J. Electrochem. Soc.*, vol. 162, no. 5, pp. A5054–A5059, 2015.

[6] C. Masarapu, H. F. Zeng, K. H. Hung, and B. Wei, "Effect of temperature on the capacitance of carbon nanotube supercapacitors," *ACS Nano*, vol. 3, no. 8, pp. 2199–2206, Aug. 2009.

[7] N. Kularatna, *Energy Storage Devices for Electronic Systems: Rechargeable Batteries and Supercapacitors*. New York, NY, USA: Academic, 2014.

[8] Y. J. Kang, H. Chung, C.-H. Han, and W. Kim, "All-solid-state flexible supercapacitors based on papers coated with carbon nanotubes and ionic-liquid-based gel electrolytes," *Nanotechnology*, vol. 23, no. 6, Feb. 2012, Art. no. 065401.

[9] A. Lamberti, M. Serrapede, G. Ferraro, M. Fontana, F. Perrucci, S. Bianco, A. Chiolerio, and S. Bocchini, "All-SPEEK flexible supercapacitor exploiting laser-induced graphenization," *2D Mater.*, vol. 4, no. 3, Jul. 2017, Art. no. 035012.

[10] Y. Xu, L. Hou, H. Zhao, S. Bi, L. Zhu, and Y. Lu, "Alumina sandpaper-supported nickel nanocoatings and its excellent application in non-enzymatic glucose sensing," *Appl. Surf. Sci.*, vol. 463, pp. 1028–1036, Jan. 2019.

[11] Z. Niu, W. Zhou, J. Chen, G. Feng, H. Li, W. Ma, J. Li, H. Dong, Y. Ren, D. Zhao, and S. Xie, "Compact-designed supercapacitors using free-standing single-walled carbon nanotube films," *Energy Environ. Sci.*, vol. 4, no. 4, p. 1440, 2011.

[12] X. Lu, D. Zheng, T. Zhai, Z. Liu, Y. Huang, S. Xie, and Y. Tong, "Facile synthesis of large-area manganese oxide nanorod arrays as a high-performance electrochemical supercapacitor," *Energy Environ. Sci.*, vol. 4, no. 8, p. 2915, 2011.

[13] L. Bao, J. Zang, and X. Li, "Flexible Zn_2SnO_4/MnO_2 core/shell nanocable-carbon microfiber hybrid composites for high-performance supercapacitor electrodes," *Nano Lett.*, vol. 11, no. 3, pp. 1215–1220, Mar. 2011.

[14] X.-L. Hu, G.-M. Hou, M.-Q. Zhang, M.-Z. Rong, W.-H. Ruan, and E. P. Giannelis, "A new nanocomposite polymer electrolyte based on poly(vinyl alcohol) incorporating hypergrafted nano-silica," *J. Mater. Chem.*, vol. 22, no. 36, p. 18961, 2012.

[15] H. Yu, J. Wu, L. Fan, Y. Lin, K. Xu, Z. Tang, C. Cheng, S. Tang, J. Lin, M. Huang, and Z. Lan, "A novel redox-mediated gel polymer electrolyte for high-performance supercapacitor," *J. Power Sour.*, vol. 198, pp. 402–407, Jan. 2012.

[16] H. Gao and K. Lian, "Advanced proton conducting membrane for ultra-high rate solid flexible electrochemical capacitors," *J. Mater. Chem.*, vol. 22, no. 39, 2012, Art. no. 21272.

[17] C.-W. Huang, C.-A. Wu, S.-S. Hou, P.-L. Kuo, C.-T. Hsieh, and H. Teng, "Gel electrolyte derived from poly(ethylene glycol) blending poly(acrylonitrile) applicable to roll-to-roll assembly of electric double layer capacitors," *Adv. Funct. Mater.*, vol. 22, no. 22, pp. 4677–4685, Nov. 2012.

[18] S.-K. Kim, H.-J. Koo, A. Lee, and P. V. Braun, "Selective wetting-induced micro-electrode patterning for flexible micro-supercapacitors," *Adv. Mater.*, vol. 26, no. 30, pp. 5108–5112, Aug. 2014.

[19] Y. Song, X.-X. Chen, J.-X. Zhang, X.-L. Cheng, and H.-X. Zhang, "Freestanding micro-supercapacitor with interdigital electrodes for low-power electronic systems," *J. Microelectromech. Syst.*, vol. 26, no. 5, pp. 1055–1062, Oct. 2017.

[20] D. Pech, M. Brunet, H. Durou, P. Huang, V. Mochalin, Y. Gogotsi, P.-L. Taberna, and P. Simon, "Ultrahigh-power micrometre-sized supercapacitors based on onion-like carbon," *Nature Nanotech*, vol. 5, no. 9, pp. 651–654, Sep. 2010.

[21] M. Beidaghi and C. Wang, "Micro-supercapacitors based on interdigital electrodes of reduced graphene oxide and carbon nanotube composites with ultrahigh power handling performance," *Adv. Funct. Mater.*, vol. 22, no. 21, pp. 4501–4510, Nov. 2012.

[22] M. S. Kim, B. Hsia, C. Carraro, and R. Maboudian, "Flexible micro-supercapacitors with high energy density from simple transfer of photoresist-derived porous carbon electrodes," *Carbon*, vol. 74, pp. 163–169, Aug. 2014.

[23] J. Lin, C. Zhang, Z. Yan, Y. Zhu, Z. Peng, R. H. Hauge, D. Natelson, and J. M. Tour, "3-dimensional graphene carbon nanotube carpet-based microsupercapacitors with high electrochemical performance," *Nano Lett.*, vol. 13, no. 1, pp. 72–78, Jan. 2013.

[24] G. Wang, V. Babaahmadi, N. He, Y. Liu, Q. Pan, M. Montazer, and W. Gao, "Wearable supercapacitors on polyethylene terephthalate fabrics with good wash fastness and high flexibility," *J. Power Sour.*, vol. 367, pp. 34–41, Nov. 2017.

[25] J. B. In, B. Hsia, J.-H. Yoo, S. Hyun, C. Carraro, R. Maboudian, and C. P. Grigoropoulos, "Facile fabrication of flexible all solid-state micro-supercapacitor by direct laser writing of porous carbon in polyimide," *Carbon*, vol. 83, pp. 144–151, Mar. 2015.

[26] V. Strong, S. Dubin, M. F. El-Kady, A. Lech, Y. Wang, B. H. Weiller, and R. B. Kaner, "Patterning and electronic tuning of laser scribed graphene for flexible all-carbon devices," *ACS Nano*, vol. 6, no. 2, pp. 1395–1403, Feb. 2012.

[27] T. Malik, S. Naveed, M. Muneer, and M. A. Mohammad, "Fabrication and characterization of laser scribed supercapacitor based on polyimide for energy storage," in *Key Engineering Materials*. Cham, Switzerland: Trans Tech, 2018, pp. 181–186.

[28] S. Naveed, T. Malik, M. Muneer, and M. Ali Mohammad, "A laser scribed graphene oxide and polyimide hybrid strain sensor," *Key Eng. Mater.*, vol. 778, pp. 169–174, Sep. 2018.

[29] Z. Wan, E. Streed, M. Lobino, S. Wang, R. Sang, I. Cole, D. Thiel, and Q. Li, "Laser-reduced graphene: Synthesis, properties, and applications," *Adv. Mater. Technol.*, vol. 3, no. 4, 2018, Art. no. 1700315.

[30] X. You, M. Misra, S. Gregori, and A. K. Mohanty, "Preparation of an electric double layer capacitor (EDLC) using miscanthus-derived biocarbon," *ACS Sustain. Chem. Eng.*, vol. 6, no. 1, pp. 318–324, Jan. 2018.

[31] Z. S. Wu, K. Parvez, X. Feng, and K. Müllen, "Graphene-based in-plane micro-supercapacitors with high power and energy densities," *Nature Commun.*, vol. 4, Sep. 2013, Art. no. 2487.

[32] B. Song, L. Li, Z. Lin, Z.-K. Wu, K.-S. Moon, and C.-P. Wong, "Water-dispersible graphene/polyaniline composites for flexible micro-supercapacitors with high energy densities," *Nano Energy*, vol. 16, pp. 470–478, Sep. 2015.

[33] Y. Lin, Y. Gao, and Z. Fan, "Printable fabrication of nanocoral-structured electrodes for high-performance flexible and planar supercapacitor with artistic design," *Adv. Mater.*, vol. 29, no. 43, Nov. 2017, Art. no. 1701736.

[34] M. D. Stoller, S. Park, Y. Zhu, J. An, and R. S. Ruoff, "Graphene-based ultracapacitors," *Nano Lett.*, vol. 8, no. 10, pp. 3498–3502, Oct. 2008.

[35] S. Wang, B. Hsia, C. Carraro, and R. Maboudian, "High-performance all solid-state micro-supercapacitor based on patterned photoresist-derived porous carbon electrodes and an ionogel electrolyte," *J. Mater. Chem. A*, vol. 2, no. 21, pp. 7997–8002, Feb. 2014.

[36] T. R. Kuphaldt, *Lessons in Electric Circuits: Direct Current*, vol. 1, 5th ed. London, U.K.: Koros Press, 2006.

[37] G. Heiland, "Surface conductivity of semiconductors and its variation by adsorption, transverse electric fields and irradiation," *Discuss. Faraday Soc.*, vol. 28, pp. 168–182, Jun. 1959.
[38] B.-A. Mei, O. Munteshari, J. Lau, B. Dunn, and L. Pilon, "Physical interpretations of nyquist plots for EDLC electrodes and devices," *J. Phys. Chem. C*, vol. 122, no. 1, pp. 194–206, Jan. 2018.
[39] R. W. Laity, "Diffusion of ions in an electric field1," *J. Phys. Chem.*, vol. 67, no. 3, pp. 671–676, Mar. 1963.

FARHEEN NASIR received the B.S. degree (Hons.) in electronics engineering from the Sir Syed University of Engineering and Technology, Pakistan, in 2016, and the M.S. degree (Hons.) in nanoscience and engineering from the National University of Sciences and Technology, Pakistan, in 2019.

She is currently a Lecturer and a Researcher with the Karachi Institute of Economics and Technology (KIET), Karachi, Pakistan. Her research interests include supercapacitors, surface acoustic wave devices, MEMS sensors, and molecular machines.

MOHAMMAD ALI MOHAMMAD received the B.Sc. degree in electrical engineering and the Ph.D. degree in electrical and computer engineering from the University of Alberta, Edmonton, AB, Canada, in 2008 and 2013, respectively.

He worked at Tsinghua University, China, as a Postdoctoral Fellow, from 2013 to 2016, where his research interests included the fabrication and testing of resistive memory devices and surface acoustic wave devices. In 2016, he joined the National University of Sciences and Technology (NUST), Islamabad, Pakistan, as a Faculty Member, where he has been working on flexible electronics. He is currently the Research Director with NUST. He majored in microsystems and nanodevices with research focus on electron beam lithography, nanomechanical sensors, and molecular dynamics simulations.